THE ASTROPHYSICAL JOURNAL, 538:505–516, 2000 August 1

A DETERMINATION OF THE HUBBLE CONSTANT USING MEASUREMENTS OF X-RAY EMISSION AND THE SUNYAEV-ZELDOVICH EFFECT AT MILLIMETER WAVELENGTHS IN THE CLUSTER ABELL 1835

P. D. MAUSKOPF,[1] P. A. R. ADE,[2] S. W. ALLEN,[3] S. E. CHURCH,[4] A. C. EDGE,[3] K. M. GANGA,[5] W. L. HOLZAPFEL,[6] A. E. LANGE,[7] B. K. ROWND,[1] B. J. PHILHOUR,[7] AND M. C. RUNYAN[7]

Received 1999 April 5; accepted 2000 February 9

ABSTRACT

We present a determination of the Hubble constant and central electron density in the cluster Abell 1835 ($z = 0.2523$) from measurements of X-ray emission and millimeter-wave observations of the Sunyaev-Zeldovich (S-Z) effect with the Sunyaev-Zeldovich Infrared Experiment (SuZIE) multifrequency array receiver. Abell 1835 is a well studied cluster in the X-ray with a large central cooling flow. Using a combination of data from *ROSAT* PSPC and HRI images and millimeter wave measurements we fit a King model to the emission from the ionized gas around Abell 1835 with $\theta_0 = 0'.22 \pm 0'.02$ and $\beta = 0.58 \pm 0.02$. Assuming the cluster gas to be isothermal with a temperature of $9.8^{+2.3}_{-1.3}$ keV, we find a y-parameter of $4.9 \pm 0.6 \times 10^{-4}$ and a peculiar velocity of 500 ± 1000 km s^{-1} from measurements at three frequencies, 145, 221, and 279 GHz. Combining the S-Z measurements with X-ray data, we determine a value for the Hubble constant of $H_0 = 59^{+38}_{-28}$ km s^{-1} Mpc^{-1} and a central electron density for Abell 1835 of $n_{e0} = 5.64^{+1.61}_{-1.02} \times 10^{-2}$ cm^{-3} assuming a standard cosmology with $\Omega_m = 1$ and $\Omega_\Lambda = 0$. The error in the determination of the Hubble constant is dominated by the uncertainty in the temperature of the X-ray emitting cluster gas.

Subject headings: cosmology: observations — distance scale — galaxies: clusters: individual (A1835) — radio continuum: galaxies — X-rays: galaxies

1. INTRODUCTION

One of the ways of understanding the distribution of matter in the universe on the largest scales is with observations of clusters of galaxies. Most of the baryonic matter in galaxy clusters is in the form of hot (several keV), intracluster (IC) gas. This gas emits X-rays and distorts the spectrum of the cosmic microwave background (CMB) through the Sunyaev-Zeldovich (S-Z) effect (Sunyaev & Zeldovich 1972). The combination of X-ray and S-Z measurements can be used to determine cluster baryon fractions, the angular diameter distances, d_A, to clusters and a value for the Hubble constant, and cluster peculiar velocities.

There is now a large sample of clusters with high signal-to-noise X-ray images and spectra from *ROSAT* and *ASCA* observations (e.g., Ebeling et al. 1996; Voges et al. 1999). These data are beginning to be combined with initial S-Z surveys of the brightest X-ray sources to obtain values for the Hubble constant and baryon fraction (see, e.g., Birkinshaw 1999). The SuZIE experiment has obtained data for $\sim$20 clusters at millimeter wavelengths in observations at the Caltech Submillimeter Observatory (CSO). Measurements at these wavelengths allow the separation of the thermal and kinetic S-Z effects and complement surveys at lower frequencies. In this paper, we present the results from an analysis of the X-ray and mm-wave measurements of Abell 1835, one of the most luminous clusters in the *ROSAT* catalog and the first cluster observed with both the SuZIE I and SuZIE II instruments. The tools developed for this analysis will be applied to the full data set of clusters observed with SuZIE II. In § 2, we describe the X-ray data and analysis. In § 3, we describe the millimeter-wave measurements. In § 4, we discuss the analysis of the millimeter-wave data and present results from the combination of these data and the X-ray data. Section 5 discusses sources of error, caveats, and directions for the future.

2. X-RAY ANALYSIS

The surface brightness of the X-ray emission scales with the density of the gas squared integrated along the line of sight,

$$B_X \propto \int n_e^2 \, d\ell \propto n_{e0}^2 \, r_0 \, , \tag{1}$$

where n_{e0} is the central electron density calculated for a gas distribution model and r_0 is a measure of the cluster diameter along the line of sight. The spectrum of emission can be used to determine the temperature of the gas while the angular distribution of X-ray emission can be used to determine the density profile. The canonical model for the density and temperature distribution of ionized gas in a cluster is a spherically symmetric, isothermal King model:

$$n_e(r) = n_{e0}\left[1 + \left(\frac{r}{r_0}\right)^2\right]^{-3\beta/2} . \tag{2}$$

X-ray observations from *ROSAT* and *ASCA* have made it possible to study the properties of cluster gas in detail and to characterize deviations from this model.

One of the features of many clusters is the presence of a large central spike in the X-ray emission. This central emission can be attributed to a central density enhancement

[1] Department of Physics and Astronomy, University of Massachusetts, Amherst, MA 01003.
[2] Department of Physics, Queen Mary and Westfield College, Mile End Road, London, E1 4NS, UK.
[3] Institute of Astronomy, Madingley Road, Cambridge, CB3 0HA, UK.
[4] Department of Physics, Stanford University.
[5] Infrared Processing and Analysis Center.
[6] Department of Physics, University of California, Berkeley.
[7] Department of Physics, Math, and Astronomy, California Institute of Technology, Pasadena, CA 91125.

called a cooling flow. Measurements suggest that cooling flow clusters are the most dynamically relaxed systems and that the assumptions of smooth gas distribution and spherical symmetry are satisfied in these systems (Allen 1997). Abell 1835 is a well studied cluster at X-ray and optical wavelengths with a large cooling flow. It is also one of the most luminous X-ray clusters in the *ROSAT* all sky survey with a luminosity of $L_X = 3.8 \times 10^{45}$ ergs s^{-1} in the 2–10 keV band.

Abell 1835 was the object of two pointed observations with the *ROSAT* PSPC, of 2542 s and 6171 s duration and one observation with the HRI of 2835 s duration. The HRI and PSPC images of Abell 1835 are shown in Figures 1 and 2 with the beam profiles of the *ROSAT* PSPC, HRI, and SuZIE. It is evident from these images that Abell 1835 has no associated subclusters or X-ray point sources within a $10' \times 10'$ field of view around the cluster. A detailed analysis of the temperature and density distribution of the IC gas in Abell 1835 has been published using these observations combined with spectral information from *ASCA* (Allen et al. 1996). This combination of data allows a determination of the temperature, metallicity, X-ray emissivity and cooling rate of the cluster as a function of cluster radius. The best-fit spectral model for the cluster including the central cooling flow gives a mass-weighted temperature of the cluster gas of $T_{e0} = 9.8^{+2.3}_{-1.3}$ keV (Allen & Fabian 1998).

We determine a model distribution for the IC gas in Abell 1835 in two ways: (i) we use a one-dimensional fit to deprojected data assuming spherical symmetry, and (ii) we use a two-dimensional fit to the X-ray image to take into account beam effects and cluster ellipticity. For the first method, the X-ray surface brightness distribution is deprojected using a standard algorithm (Fabian et al. 1981) to obtain values for the electron density as a function of cluster radius (Allen et al. 1996). The results from both the HRI and PSPC deprojections are plotted in Figure 3 where the electron densities have been calculated assuming a Hubble constant of $H_0 = 50$ km s^{-1} Mpc^{-1} and $q_0 = 0.5$.

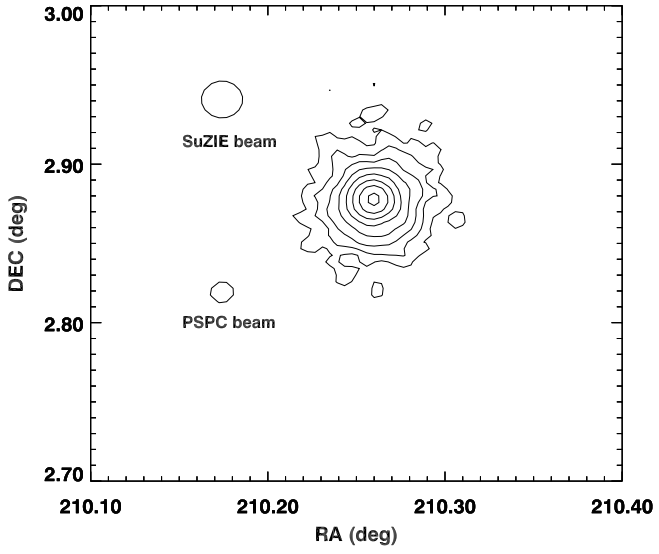

FIG. 1.—Contour image of Abell 1835 from the *ROSAT* PSPC. A pixel size of $15'' \times 15''$ has been used and the image has been smoothed with a Gaussian with FWHM 2 pixels. Contours are spaced logarithmically from 1.6×10^{-4} counts s^{-1} to 0.02 counts s^{-1}. Also shown are the half-power points of the PSPC and SuZIE PSFs.

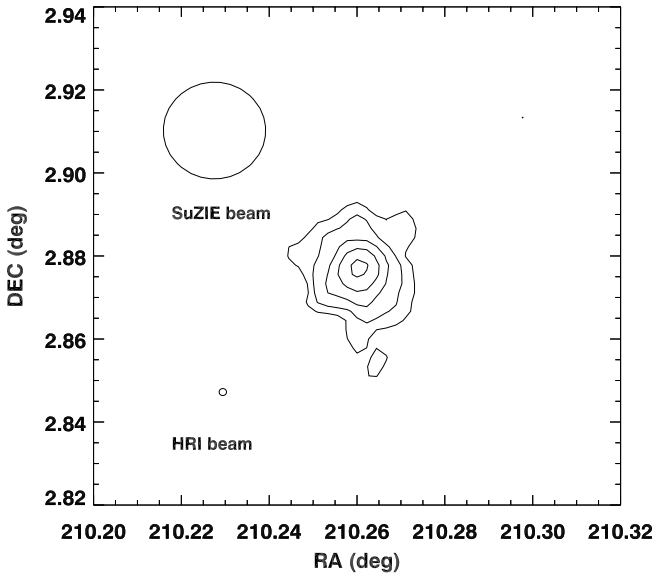

FIG. 2.—Contour image of Abell 1835 from the *ROSAT* HRI. A pixel size of $8'' \times 8''$ has been used and the image has been smoothed with a Gaussian with FWHM 2 pixels. Contours are spaced logarithmically from 3.75×10^{-4} counts s^{-1} to 0.06 counts s^{-1}. Also shown are the half-power points of the HRI and SuZIE PSFs.

We fit a simple King model to these data and obtain best-fit values for $\beta = 0.54 \pm 0.04$, $\theta_0 = 0'.20 \pm 0'.06$, and $n_{e0} = 0.052 \pm 0.002$ cm^{-3}. The χ^2 contours for the θ_0 versus β variables are shown in Figure 4. If we let the Hubble constant be a free parameter, we can solve for the product,

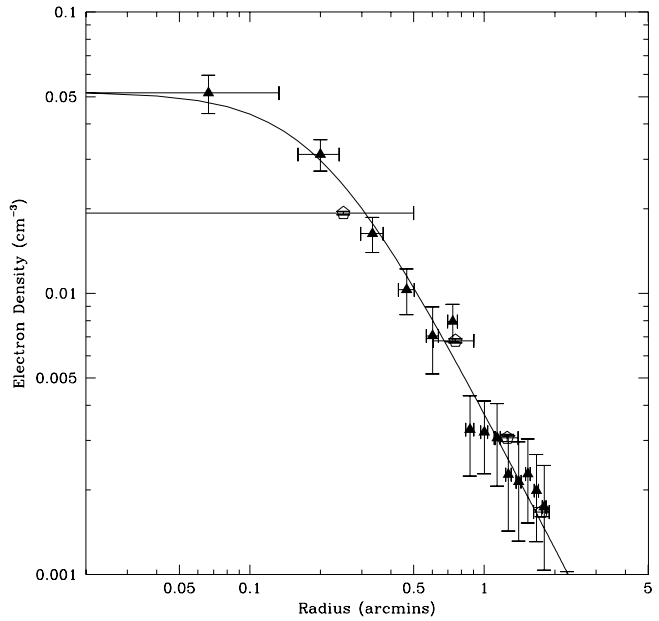

FIG. 3.—Electron density of Abell 1835 as a function of angular radius assuming a Hubble constant of $H_0 = 50$ km s^{-1} Mpc^{-1} from a deprojection of *ROSAT* HRI and PSPC images. Open hexagons represent the average electron density within circular shells spaced by 30″ as measured by the *ROSAT* PSPC, and triangles represent the average electron density within 8″ shells as measured by the *ROSAT* HRI. The line is the best-fit King model with $\theta_0 = 0'.20$, $\beta = 0.54$, and $n_{e0} = 0.052$ cm^{-3}.

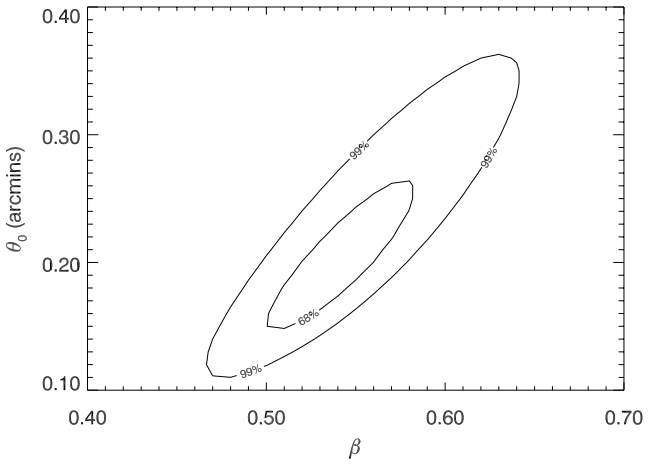

FIG. 4.—Chi-squared contours of probability for fitting a King model with parameters θ_0 and β to the deprojected electron density distribution in Abell 1835. Models were fitted to a combination of deprojected data from the HRI and PSPC images.

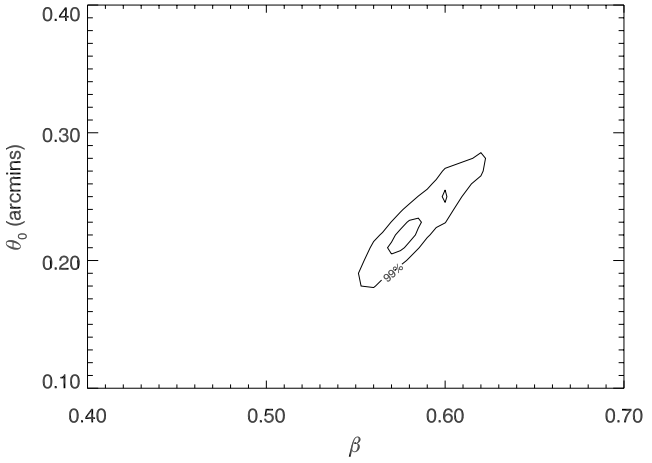

FIG. 5.—Chi-squared contours of probability for fitting source models to the PSPC images of Abell 1835. The two-dimensional source models were generated by convolving the PSF of the PSPC with King models, varying the parameters θ_0 and β.

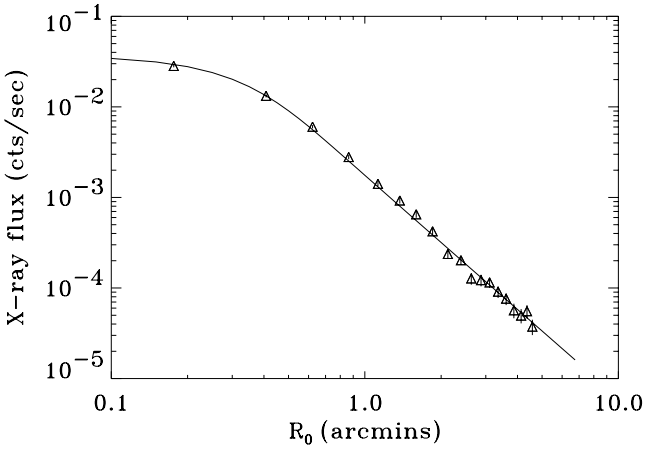

FIG. 6.—X-ray flux vs. radius from PSPC images of Abell 1835. Points represent average flux in rings spaced by 15″ in diameter around the cluster centroid. The line shows the radial profile of the best-fit King model ($\theta_0 = 0.'22$, $\beta = 0.575$) convolved with the PSPC beam.

$n_{e0}^2 d_A$:

$$n_{e0}^2 d_A = 8.47^{+0.67}_{-0.64} \times 10^{24} \text{ cm}^{-5} . \quad (3)$$

We exclude the innermost point with $r < 0.1$ Mpc ($H_0 = 50$ km s^{-1} Mpc^{-1}) of the deprojected PSPC data from the fit because the PSPC deprojection does not account for the finite resolution of the PSPC.

In addition we make two-dimensional fits to the PSPC and HRI images to determine θ_0 and β and estimate the cluster ellipticity. We find the X-ray centroid, (x_0, y_0) and define an "image radius" as a function of orientation angle:

$$r_i(\alpha) = \frac{\int F_X(r,\phi)|\cos(\phi(x,y) - \alpha)| r^2 dr\, d\phi}{\int F_X(r,\phi) r\, dr\, d\phi} , \quad (4)$$

where $r = 0$ at the X-ray centroid and $F_X(r, \phi)$ is the X-ray flux. For a circular image, $r_i(\alpha)$ is a constant. For an ellipse, $r_i(\alpha) = a(1 + \epsilon \sin \alpha)$, where ϵ is the ellipticity, $\epsilon = (a - b)/a$.

Abell 1835 is almost circular with $\epsilon = 8\% \pm 2\%$, where the error is due to the pixelization of the images. We generate models for a grid of values of θ_0 and β and convolve each model with the PSF of both the HRI and PSPC instruments. For the PSPC, we use the hard-band 0.4–2.0 keV image and the PSF model of Hasinger et al. (1992), which has a FWHM $\sim 25''$ at the center of the image. For the HRI, we use a Gaussian PSF with a 5″ FWHM. One and two sigma contours for the King model parameters θ_0 and β are shown in Figure 5. The best-fit parameters are $\beta = 0.58^{+0.01}_{-0.02}$ and $\theta_0 = 0.'22^{+0.02}_{-0.02}$. The error in θ_0 is a combination of statistical noise and the cluster ellipticity that gives $\Delta\theta_0 = \pm\epsilon\theta_0/2 = \pm 0.'008$. Figure 6 shows the X-ray flux from the PSPC images averaged in 15″ rings around the image centroid compared to the best-fit model. The χ^2 of the fit is 15 for 16 degrees of freedom. We use Gaussian statistics in this analysis because each bin contains more than 100 counts.

3. MILLIMETER-WAVE DATA

The dominant source of millimeter-wave radiation from clusters of galaxies is from the Sunyaev-Zeldovich (S-Z) effect (Sunyaev & Zeldovich 1972), a distortion of the spectrum of the cosmic microwave background (CMB) due to its interaction with the IC gas. The S-Z effect has a thermal component due to the transfer of energy from the hot gas to the CMB and a kinematic component due to the bulk motion of the cluster with respect to the CMB rest frame. The brightness of each component is proportional to the density of the IC gas integrated through the line of sight, $B_{S\text{-}Z} = yI_0\, g(x)$, where $I_0 = 2(kT_0)^3/h^2c^2$, $y \propto \int n_e d\ell \propto n_{e0} d_A$ is the dimensionless Compton y-parameter and $g(x)$ is a frequency-dependent scaling ($x = h\nu/kT$). The spectrum of the S-Z kinetic effect is given by

$$g_K(x) = h(x) \frac{v_p}{c\gamma_e} , \quad (5)$$

where v_p is the cluster peculiar velocity, $\gamma_e \equiv kT_e/m_e c^2$ is the normalized gas temperature and

$$h(x) = \frac{x^4 e^x}{(e^x - 1)^2} . \quad (6)$$

The spectrum of the S-Z thermal effect is given by

$$g_T(x) = h(x)[x \tanh(x) - 4] . \quad (7)$$

For a King model gas distribution with temperature, T_e, central density, n_{e0}, core radius, r_c, and power-law parameter, β, the central Comptonization, y_0 is

$$y_0 = n_{e0}\, d_A\, \sigma_T \left(\frac{kT_e}{m_e c^2}\right) \theta_0\, B\left(\frac{1}{2}, \frac{3\beta}{2} - \frac{1}{2}\right), \qquad (8)$$

where $B(\frac{1}{2}, (3\beta/2) - \frac{1}{2})$ is the incomplete beta function. Estimation of v_p requires measurements of the S-Z effect at a variety of wavelengths and a determination of the IC gas temperature but is insensitive to cluster morphology or asphericity.

The millimeter-wave data presented in this paper were obtained with the SuZIE I and SuZIE II receivers at the Caltech Submillimeter Observatory (CSO). The rest of this section describes these measurements and the data processing performed to obtain values for the cluster y-parameter and peculiar velocity.

3.1. *Instrument*

The SuZIE receivers are designed for ground-based millimeter-wave continuum measurements from the Caltech Submillimeter Observatory (CSO) on Mauna Kea in Hawaii. The techniques and instrumentation developed for the SuZIE receivers have been described in detail (Holzapfel et al. 1997a; Mauskopf et al. 2000). Each consists of a focal plane array of Winston horns which overilluminate a cold (2 K) Lyot stop at an image of the primary mirror formed by a warm tertiary mirror. This optical design produces matching illumination patterns on the primary mirror that separate slowly through the atmosphere to form 1.′4–1.′7 beams, separated by up to 5′ on the sky. Differences between the signals form effective chop throws of 2.′1–5′ on the sky. These beams are drift scanned by 30′ over the known X-ray positions of clusters of galaxies to produce a one-dimensional slice through the cluster with each row of detectors. The different specifications of the SuZIE I and SuZIE II receivers are detailed in the data analysis sections.

3.2. *Scan Strategy*

We employ drift scans for SuZIE measurements to minimize spurious sources of noise due to motion of the telescope or modulation of the beam. Immediately before each scan, the telescope tracks a point on the sky offset from the source position by a fixed angle in right ascension and declination: $(\alpha_0, \delta_0) = (\alpha_{\rm source} + {\rm RAO}, \delta_{\rm source} + {\rm DECO})$. At the same time, a Dewar rotator aligns the array so that the widely spaced pixels are aligned parallel to the direction of sky rotation. The telescope pointing system then stops tracking in R.A., sends a synchronization pulse to the data computer to initiate data storage and remains fixed with respect to the earth for the 120 s long scan duration. The DECO is chosen to be $\pm 60''$ so that the center of the source will pass through one of the rows of photometers spaced by 120″. The RAO is set to $-720''$ and $-1080''$ on alternating scans so that the source position within the scan alternates around the center of the scan. A scan-synchronous instrumental baseline can be removed by differencing sequential scans without removing a significant amount of signal from the source.

3.3. *Sources*

We select source clusters for S-Z observations based on four factors: X-ray luminosity and temperature, angular size, and sky position. High X-ray luminosities imply a combination of high electron density and temperature in the cluster gas so that these clusters should also have relatively large y-parameters. If the IC gas is distributed according to a King model, the S-Z brightness falls off relatively slowly with radius and has a significant surface brightness out to several core radii. The 1.′4 beam size and 4.′2 beam throw in the SuZIE instrument motivate us to select clusters with apparent diameters, $\theta_c \sim 1.'4$, corresponding to cluster redshifts, $z \geq 0.1$. Because measurements of several hours each night for several nights are needed for these observations, we select clusters with declination near the latitude of the CSO $\sim +20°$.

We chose to observe Abell 1835 (R.A. $= 14^{\rm h}1^{\rm m}2^{\rm s}$, Decl. $= 2°52'41''$) with the SuZIE II receiver for several reasons. First, we knew it was a bright S-Z source from a detection of the S-Z thermal effect in 8 hr of integration on 1994 April 5–11 with the SuZIE I receiver at 142 GHz. We used this detection as an additional calibration of the new receiver and more importantly as a check for systematic effects in both measurements. Second, we had not measured this cluster at 217 or 269 GHz and therefore had no limit on the peculiar velocity. Finally, we knew that this cluster had been well studied in the X-ray and was a good candidate for a determination of the Hubble constant. We obtained 22 hr of data on Abell 1835 at 145, 221, and 279 GHz during the period of 1996 April 17–24 with the SuZIE II instrument mounted on the CSO. During both SuZIE I and II observations, the source elevation varied from 50°–80°, and the observations consisted of drift scans of 120 s length, covering $\sim 30'$ on the sky.

3.4. *Blank Sky*

Blank sky observations are useful for determining the overall performance of the instrument and setting limits on the contribution of sources of systematic error. Two blank sky regions observed in 1994 April have been used to provide upper limits on the systematic baselines in the measurements of the clusters Abell 2163 and Abell 1689 (Holzapfel et al. 1997a, 1997b). In addition, these measurements have been used to place upper limits on the level of primordial CMB fluctuations (Church et al. 1997). We selected two regions of sky for blank sky observations during the first and last parts of the night from 1996 April 17–24. We chose regions that were free of known sources from the *IRAS* point source catalog and the Parks point source survey and that covered a similar range of elevation angles to the cluster observations. In addition, we avoided areas that had large contrast in the diffuse emission from interstellar dust as determined from 100 μm *IRAS* maps (Schlegel et al. 1998).

4. S-Z DATA ANALYSIS

The analysis of the SuZIE data involves the following steps:

1. Extract a beam map for each pixel using calibration scans made during the observation.
2. Calculate the S-Z spectral coefficients by convolving measured transmission spectra of the filters with relativistic intensity profile, calibration spectra, and atmospheric optical depth model.
3. Generate a King model for the distribution of gas using best-fit X-ray parameters θ_0 and β.

4. Generate fitting models by convolving the King model with the beam map.
5. Despike and bin the raw millimeter-wave data.
6. Co-add the binned data from all scans. Find the best-fit position and amplitude for the co-added data.
7. Fit the source model to each scan and find the best-fit amplitude using the best-fit position from 6.

In this section, we describe these steps in detail and also discuss refinements to this analysis in the case of the SuZIE II multifrequency data.

4.1. *Calibration*

Observations of planets are used to map the beam shapes of the instrument and calibrate the responsivity of the pixels. In 1994 April Uranus was used to map the beams and as a calibration source. In April of 1995 and 1996 we used scans of Uranus and Mars to calibrate the instrument and scans of Jupiter to map the beams. We assign $\pm 6\%$ uncertainty to the brightness of Uranus, and $\pm 5\%$ uncertainty to the absolute brightness of Mars (Orton et al. 1986). Rotation of the array about the optical axis causes small changes in the instrument's beam shapes. Calibration scans over the range of rotation angles at which we observed the clusters change by at most 8%. We combine these errors and assume a total calibration error of 10%. In the SuZIE I system, the beams had FWHM $\sim 1\farcm7$ and were separated by $2\farcm3$ and $4\farcm6$. For SuZIE II, the beam sizes are $1\farcm1-1\farcm5$ FWHM and the separations were $\sim 4\farcm2$. Measurements of the solid angles of each beam are given in Holzapfel et al. (1997c) and Mauskopf et al. (2000).

For S-Z observations, we integrate the best-fit King model from the X-ray data along the line of sight to find the column depth of electron gas in the cluster as a function of angle from the center:

$$N_e(\theta,\phi) = 2n_e(0)B\left(\frac{1}{2},\frac{3\beta}{2}-\frac{1}{2}\right)\theta_0 d_A \times\left(1+\frac{\theta^2+\phi^2}{\theta_0^2}\right)^{1/2-3\beta/2}, \quad (9)$$

where $B(\frac{1}{2},(3\beta/2)-\frac{1}{2})$ is the incomplete beta function, $\theta_0 = r_0/d_A$ and d_A is the angular diameter distance to the cluster. The S-Z signal we expect as a function of position on the sky is the convolution of the electron optical depth as a function of angle with the beam pattern measured by calibrating on a planet:

$$\mathrm{V}_{\mathrm{model}}(\theta) = \frac{I_{\mathrm{S\text{-}Z}}}{I_P}\frac{1}{\Omega_P}\int V_P(\theta-\theta',\phi')\frac{N_e(\theta',\phi')}{N_e(0)}d\theta'\,d\phi', \quad (10)$$

where Ω_P is the solid angle subtended by the planet, $V_P(\theta, \phi')$ is the voltage out from the calibration scan. We calculate beam models corresponding to the expected signal from a cluster passing through the array for values of θ_0 and β within the limits allowed by the X-ray data.

4.2. *SuZIE I Data*

4.2.1. *Raw Data Reduction*

SuZIE I contained six bolometers arranged in two rows of 3 pixels with $1\farcm7$ beams. The data from SuZIE I observations consist of six single channels and six differential channels. The single channels measure the total power on each detector with low gain and are dominated by total power sky temperature fluctuations. If we define the bolometers in a row as S1, S2, and S3, the differential channels are equivalent to: D12 = S1 − S2, D23 = S2 − S3, and D31 = S3 − S1 (see Fig. 7). The differential signals are dominated by differential sky temperature variations. The three differences between bolometers in a row produce beam patterns on the sky with beam separations of $2\farcm3$ for D12 and D23 and $4\farcm6$ for D31. These three measurements are not independent; for example, D31 = −(D12 − D23). To remove this degeneracy, we produce a triple beam chop, T123 = D12 + D23, in software that can be used as a measurement independent to D31. For each scan, the raw data are cleaned of cosmic-ray spikes and binned into $0\farcm75$ bins.

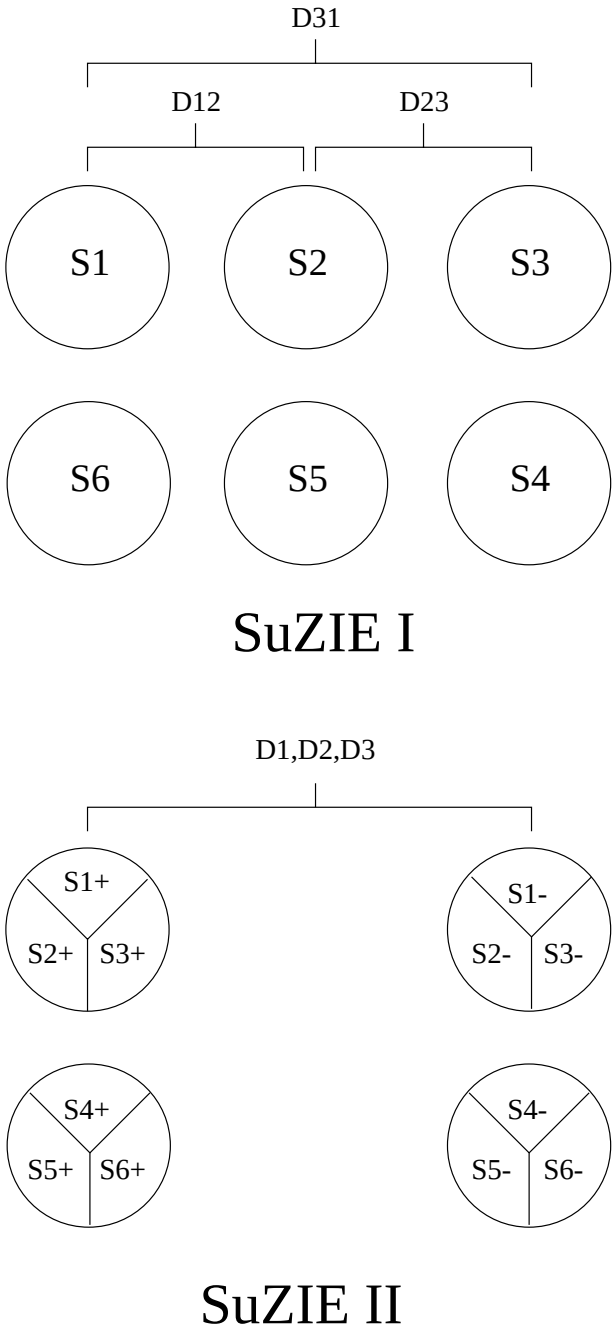

FIG. 7.—Positions and labels for the beams on the sky in SuZIE I and SuZIE II. In SuZIE I, a single bolometer is associated with each pixel and measures incoming radiation at a single frequency, either at 145, 221 or 279 GHz, while in SuZIE II, each pixel has three bolometers which measure all three bands simultaneously.

4.2.2. *Co-added Data*

The co-added data are calculated from a weighted average of each binned scan with an offset, slope and single channel model removed using a procedure described in detail in Holzapfel et al. (1997a). Co-added 142 GHz data for observations of Abell 1835 from 1994 with the 4.′6 chop for the double and triple beam chop centered on the source are shown in Figures 8 and 9.

We fit a beam model to the co-added data and let the center of the cluster and the model amplitude vary over the scan. We calculate the chi-squared distribution of the fit as a function of cluster position and amplitude, and for further analysis, fix the cluster position at the point with the minimum chi-squared. For Abell 1835, we find $y_0 = 5.0 \pm 0.4 \times 10^{-4}$ with the best-fit position $\phi_0 = -0.'1^{+0.1}_{-0.15}$ from the X-ray center of the cluster. The χ^2 of the best-fit model to the co-added data is $\chi^2 = 206.7$ for 192 degrees of freedom.

4.2.3. *Single Scan Fits*

We also fit the X-ray determined source model to each scan and calculate the mean and the dispersion in the fit amplitudes. The best-fit amplitude for the source model is found by minimizing the χ^2 of the data from the four independent measurements corresponding to the single difference, D3, and triple beam chop, T123 in both R.A. offsets. The signal-to-noise in the D6 and T456 measurements is negligible compared to the D3 and T123 signals because the core radius of Abell 1835 is much smaller than the separation in DEC between rows. This analysis avoids problems in the error estimation due to noise correlations between points in a scan since the shape of the sky noise is independent from scan to scan. Using this method, we find a y-parameter value from the 1994 April, 142 GHz data of $y_0 = 4.86 \pm 0.43 \times 10^{-4}$. Table 1 shows the results from scan-to-scan fits for each of the four independent data sets.

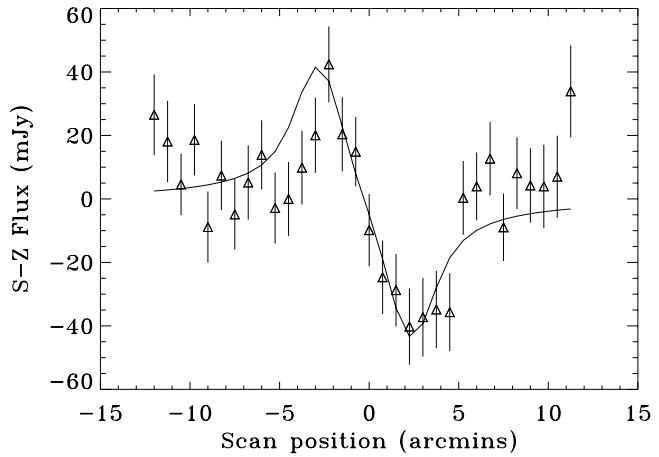

FIG. 8.—Co-added data from channel D3 during the observation of Abell 1835 with SuZIE I at 142 GHz. This channel consists of the difference between two beams with FWHM $\sim 1.'7$ separated by $\sim 4.'4$. The curve corresponds to a central Comptonization of $y_0 = 4.5 \times 10^{-4}$.

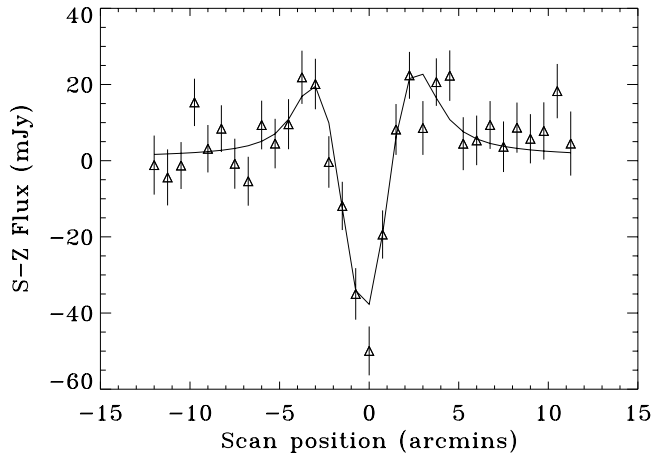

FIG. 9.—Abell 1835 with SuZIE I at 142 GHz. This channel consists of a triple beam chop with three $1.'7$ FWHM pixels in a row with center to center spacing of $2.'2$. The curve corresponds to a central Comptonization of $y_0 = 5.5 \times 10^{-4}$.

The value for the y-parameter in Abell 1835 and the error in this value are consistent using either the scan-to-scan fits or the co-added data, however, the measurements from the triple beam chop, T123, and the double beam chop, D3, are statistically different from each other. There are several possible explanations. The D3 data have overall higher noise and is more affected by non-Gaussian atmospheric fluctuations than the T123 data. However, non-Gaussian noise from cosmic rays will affect the T123 data more because the T123 signal has a higher hit rate since it is made from three bolometers instead of two bolometers and the T123 cluster model is more similar to a cosmic-ray event than the D3 model. Finally, the T123 signal will appear large relative to the D3 signal if the model for the gas distribution derived from the X-ray data overestimates the core radius of the cluster.

4.3. *SuZIE II Data*

SuZIE II contains 12 bolometers mounted in four photometers, each with three channels at 145, 220 and 271/355 GHz. These bands are designed to measure the spectrum of the Sunyaev-Zeldovich effect in distant clusters of galaxies while providing improved rejection of differential atmospheric noise. The photometers have entrance feed horns that define four $1.'4$ beams on the sky. The photometers are labeled A+, A−, B+, B−, where the spacing

TABLE 1

y-PARAMETER ESTIMATES FROM SCAN-TO-SCAN FITS TO 142 GHz MEASUREMENTS OF ABELL 1835

Channel	RAO (arcsec)	y_0 ($\times 10^{-4}$)	σ_y ($\times 10^{-4}$)
D3	1080	3.14	1.11
D3	720	3.59	0.99
T123	1080	5.60	0.79
T123	720	5.65	0.76
D6	1080	3.47	3.71
D6	720	7.03	3.00
T456	1080	7.17	5.53
T456	720	3.14	5.00
Total.....		4.86	0.43

NOTES.—Values are given for each independent data set from the array of six detectors: D3 and D6 correspond to dual beam differences and T123 and T456 correspond to triple beam chops. Channels 1, 2, and 3 were centered on the source, and channels 4, 5, and 6 were offset by 2′ in declination. The total is calculated from a fit to all four independent measurements simultaneously in each offset, with each measurement weighted by its individual dispersion given in the table.

between A+ and A− and between B+ and B− is 4.2, while the spacing between A+ and B+ and between A− and B− is 2.1 (see Fig. 7).

4.3.1. *Raw Data Reduction*

The SuZIE II data are cleaned and binned using the same procedure as for the SuZIE I data. The cosmic-ray spikes in the raw data occur about once in every 10 scans rather than once every scan because the SuZIE II bolometers have a smaller cross section to cosmic rays than the SuZIE I bolometers (Mauskopf et al. 1997).

4.3.2. *Spectral Correlation Analysis*

We analyze the SuZIE II data in several different ways. First, we treat the frequency bands as independent and calculate model amplitudes and errors at each frequency. During the observations in 1996 April, the average sky noise was about 3 times larger than in 1994 April, so the raw data have significantly worse signal-to-noise despite more than twice the integration time. Measurements with SuZIE I at each frequency were made far enough apart in time (months) so that they were uncorrelated. However, both the amplitudes and errors in the fits to the SuZIE II data are correlated because the dominant source of noise at each frequency is differential sky temperature fluctuations.

We can remove much of the sky noise by forming linear combinations of the channels. We try several different atmospheric models. We first assume that the peculiar velocity of the cluster is negligable. In this case, we remove atmospheric noise from the 145 and 279 GHz channels by subtracting correlated signal in the 1.4 mm channel from the other channels. co-added SuZIE II 145 GHz data cleaned with the 221 GHz signal is shown in Figure 10. We also use a model that consists of a linear combination of all three frequency channels that contains no S-Z thermal or kinetic signal. We determine the coefficients of this model by solving the set of equations:

$$V_n^i = M_n[\alpha_i y_0 + \beta_i v_p] + \gamma_i A_n^i + \epsilon_i \qquad (11)$$

We calculate the parameters α_i and β_i from the integral of the spectra of the different S-Z components over the bands. We convolve the spectral energy density functions (SEDs), $I_P(\nu)$, of Uranus and Mars with the measured spectral bands of the instrument to normalize the brightness in each band:

$$\alpha_i = \frac{\int f_i(\nu) I_T(\nu) d\nu}{\int f(\nu) I_P(\nu) d\nu}, \quad \beta_i = \frac{\int f_i(\nu) I_K(\nu) d\nu}{\int f(\nu) I_P(\nu) d\nu}. \qquad (12)$$

We estimate γ_i from measured correlations between bands averaged over the observations since this is the dominant signal in the data. This analysis introduces additional correlations between the 145 and 279 GHz data and does not allow the y-parameter and peculiar velocity to be measured simultaneously.

A summary of these results for the measurement of the y-parameter is shown in Tables 2 and 3.

Finally, we determine independent amplitudes for S-Z thermal and kinetic signals in each scan by a fit to all of the data simultaneously. We define a model for each channel consisting of offset, slope, common mode temperature fluctuations, differential temperature fluctuations, and astro-

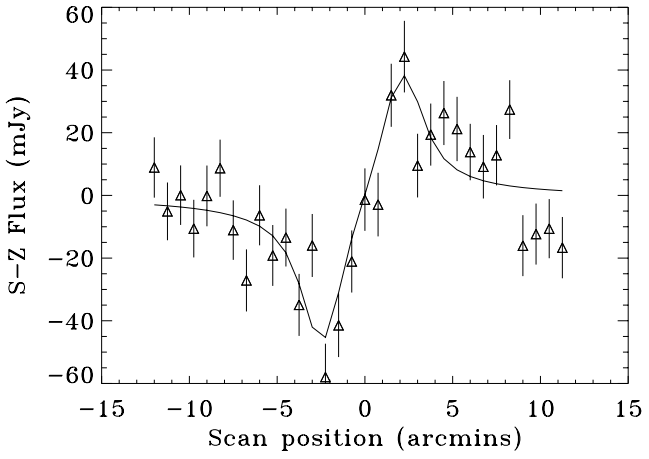

FIG. 10.—Co-added data from the 145 GHz differential channel centered on the cluster Abell 1835 during observations in 1996 April. The correlated signal in the 221 GHz channel has been removed in each scan prior to co-adding the data. The line is the 1996 beam model scaled to a y-parameter value of $y_0 = 6.0 \times 10^{-4}$.

TABLE 2

y-PARAMETER ESTIMATES FROM SCAN-TO-SCAN FITS TO 145 GHz MEASUREMENTS OF ABELL 1835

Channel	RAO (arcsec)	y_0 ($\times 10^{-4}$)	σ_y ($\times 10^{-4}$)
D3 (raw).....	1080	2.7	2.5
D3 (raw).....	720	2.8	2.8
D3 (a).....	1080	3.4	1.7
D3 (a).....	720	4.9	1.8
D3 (b)	1080	6.0	1.2
D3 (b)	720	5.4	1.3
Total (b).....		5.7	0.9

NOTES.—Values are given for the dual beam difference, D3 centered on the cluster with different models of atmospheric noise removed. The measurements marked (raw) are analyzed as single frequency measurements without making any use of the multifrequency information. Model (a) uses a linear combination of all three channels that contains no S-Z thermal or kinetic signal, and model (b) uses the 221 GHz data to clean the 145 GHz data. Conversion from signal amplitude to peculiar velocity assumes a y-parameter of 4.9×10^{-4}.

TABLE 3

PECULIAR VELOCITY ESTIMATES FROM SCAN-TO-SCAN FITS TO 221 GHz MEASUREMENTS OF ABELL 1835

Method	RAO (arcsec)	v_p (1000 km s^{-1})	σ_v (1000 km s^{-1})
D2 (raw).....	1080	5.0	2.2
D2 (raw).....	720	−2.0	2.6
D2 (a).....	1080	0.8	1.6
D2 (a).....	720	1.6	1.6
D2 (b).....	1080	1.2	0.9
D2 (b).....	720	0.7	1.0
D2−D3 mod (c).....	1080	0.8	1.4
D2−D3 mod (c).....	720	0.3	1.4
Total (c)		0.5	1.0

NOTES.—Values are given for the dual beam difference, D2 centered on the cluster with different models of atmospheric noise removed. The measurements marked (raw) are analyzed as single frequency measurements without making any use of the multifrequency information. Model (a) uses a linear combination of all three channels that contains no S-Z thermal or kinetic signal, model (b) uses a combination of 145 and 279 GHz data that has no S-Z thermal signal, and model (c) uses the SuZIE II 145 GHz data subtracting a model scaled by the best-fit to the SuZIE I data to clean the 221 GHz data.

physical signal, e.g.,

$$\boldsymbol{M}_1 = A_0 + A_1 \boldsymbol{x} + A_2 \boldsymbol{S} + A_3 \boldsymbol{\alpha}(x) + A_4 \boldsymbol{V}_{\text{model 1}}(x) , \tag{13}$$

where $\boldsymbol{S} = S1 + S2 + S3 + S4 + S5 + S6$ is the average signal from the single channels over the scan and $\boldsymbol{\alpha}(x)$ is the atmospheric model. We fix the ratio of S-Z model amplitudes in the different channels to correspond to the spectra of the S-Z thermal and kinetic effects.

The y-parameter is given by the measured amplitude of the S-Z thermal signal, and the peculiar velocity is given by the ratio of the measured amplitude of the peculiar velocity signal to the average value for the y-parameter. From the simultaneous fit to the SuZIE II data alone, we find $y_0 = 6.0 \pm 1.5 \times 10^{-4}$ and $v_p = 900 \pm 1200$ km s^{-1}. Figure 11 shows a scatter plot of the best-fit peculiar velocity and y-parameter values in each scan. We calculate the weighted density of points in this graph by multiplying each point by $1/\chi^2$ from the fit and averaging over boxes 100 km s^{-1} $\times$ $\Delta y = 4 \times 10^{-6}$. We plot 68%, 95%, and 99% likelihood contours using this probability density function.

The errors in these measurements compared to either previous results using SuZIE I data or the scan-to-scan fits in the SuZIE II data set are due to our inability to distinguish between the different spectral components in the three bands. Note that the error in the y-parameter is dominated by the correlated error in the peculiar velocity. For example, if we calculate the signal at 145 GHz:

$$\frac{\Delta T_{145}}{T} \sim y_0 \left(1 - \frac{0.175 v_p}{1000 \text{ km s}^{-1}}\right), \tag{14}$$

we find $\Delta T_{145}/T = 5.35 \pm 1.16 \times 10^{-4}$, while the error we expect from the uncertainty of $\delta v_p = 1200$ km s^{-1} is

$$\delta\left(\frac{\Delta T_{145}}{T}\right) = \frac{\delta v_p \tau}{c} = 1.0 \times 10^{-4} . \tag{15}$$

We break this degeneracy and obtain a better limit on the peculiar velocity using both the SuZIE I and SuZIE II data. We eliminate one of the free parameters in the SuZIE II data analysis by fixing the value of the 145 GHz signal to be the best-fit value from the SuZIE I data, $4.9 \pm 0.4 \times 10^{-4}$. We then solve simultaneously for the peculiar velocity and atmospheric signal using the multifrequency data and find $v_p = 500 \pm 1000$ km s^{-1}.

In more recent measurements with the SuZIE II receiver we have replaced the 1.1 mm band with a channel at 850 μm which is more sensitive to emission from the atmosphere and less sensitive to S-Z peculiar velocity signal than the 1.1 mm channel. This allows a better separation of the S-Z spectral components from the atmospheric noise, giving a simultaneous measurement of y-parameter and peculiar velocity in one observation.

4.4. *Blank Sky*

We performed the same analysis on two additional data sets acquired during the same nights, before and after the integration on Abell 1835, in areas of sky free of known sources. These blank sky data sets can be used to set a limit on the level of possible scan-synchronous systematic signals from detector microphonic response or cold stage temperature fluctuations. Blank sky data can also be used to probe the level of astrophysical confusion from unresolved point sources, extended galactic emission, and CMB anisotropies. In fact, we have used previous single frequency blank sky data to place some of the lowest upper limits on CMB anisotropy at arcminute angular scales (Church et al. 1997).

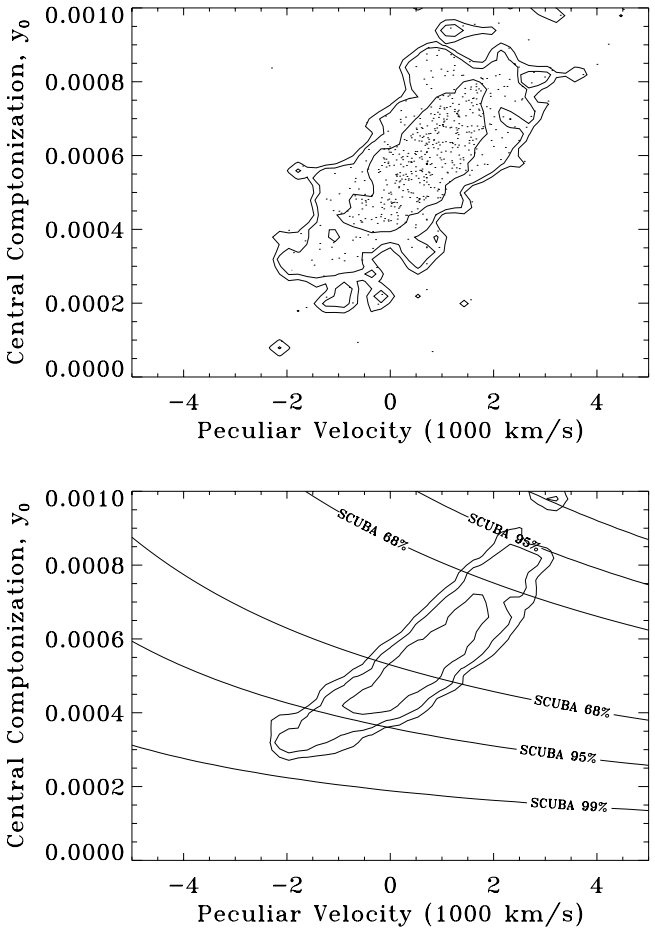

FIG. 11.—(*Top*) One, two and three sigma (68%, 95%, 99%) likelihood contours for the y-parameter and peculiar velocity from SuZIE II observations of the cluster Abell 1835 in 1996 April. The best-fit values for the SuZIE II data are $y_0 = 6.3 \pm 1.8 \times 10^{-4}$ and $v_p = 900 \pm 1500$ km s^{-1}. Points in the plot are from the fits to each scan, where the difference between the fit values and the average of all the points has been divided by the square root of the total number of points. (*Bottom*) One, two and three sigma (68%, 95%, 99%) likelihood contours for the y-parameter and peculiar velocity from a combination of SuZIE I and SuZIE II observations of the cluster Abell 1835. The best-fit values are $y_0 = 4.7 \pm 0.5 \times 10^{-4}$ and $v_p = 700 \pm 1300$ km s^{-1}. Also shown are 1, 2, and 3 σ contours from the SCUBA 850 μm detection of Abell 1835 assuming that all of the flux is from the S-Z increment. The parameters of the King model used for the fits are $\beta = 0.58$ and $\theta_c = 0'.22$, The errors in estimated y-parameter and peculiar velocity are correlated. Because the spectra of the S-Z thermal effect, the S-Z kinetic effect, and the atmosphere are only partially orthogonal, significant improvement in the rejection of atmospheric noise is obtained by fixing the value of either the y-parameter or the peculiar velocity.

We calculate the y-parameter and peculiar velocity for the two regions of blank sky observed in 1996 April. We observed Region A, centered at R.A. = $16^h30^m30^s$, Decl. = 4°0′0″ at the beginning of the night and region B, centered at R.A. = $10^h18^m30^s$, Decl. = 5°30′0″ at the end of the night. We use the amplitude of the peculiar velocity component of the signal assuming a y-parameter value equal to the best-fit value for Abell 1835 in order to calculate the contribution of the baseline peculiar velocity signal. The average baseline contributions to the measured y-

parameter and peculiar velocity in Abell 1835 are A: $y = -0.02 \pm 0.65 \times 10^{-4}$, $v_p = 400 \pm 1001$ km s^{-1}; B: $y = 0.05 \pm 0.54 \times 10^{-4}$, $v_p = -100 \pm 800$ km s^{-1}, where we have computed the y-parameters assuming no peculiar velocity component and we have computed the peculiar velocities assuming no y-parameter component. We detect no significant baseline for either the peculiar velocities or y-parameters. Combining the SuZIE I and SuZIE II data sets with the blank sky observations, we find a y-parameter of $y_0 = 4.9 \pm 0.4 \times 10^{-4}$ assuming Abell 1835 has zero peculiar velocity.

5. HUBBLE CONSTANT

In this section we combine S-Z and X-ray observations of the cluster Abell 1835 in order to determine the Hubble constant. The determination of H_0 presented here follows the prescription outlined by Birkinshaw, Hughes, & Arnaud (1991, hereafter BHA) and refined by Holzapfel et al. (1997a) for combining S-Z and X-ray measurements and accounting for sources of error.

5.1. *Isothermal Gas*

We estimate the parameters n_{e0} and d_A with measurements of (i) the cluster gas temperature distribution, $T_e(r)$, from the spectrum of X-ray emission, (ii) the cluster morphology from the X-ray or S-Z surface brightness distribution, (iii) the X-ray and S-Z flux levels, and (iv) the assumptions that the cluster is spherically symmetric and the cluster gas is smoothly distributed. The X-ray data give the product of the central electron density squared times the angular diameter distance, $n_{e0}^2 d_A$:

$$n_{e0}^2 d_A = 8.47^{+0.67}_{-0.64} \times 10^{24} \text{ cm}^{-5} , \quad (16)$$

where the error is dominated by differences in the value of the central density for the different X-ray density models allowed by the fits to the PSPC data. Assuming an isothermal gas distribution with electron temperature, $T_e = 9.8^{+2.3}_{-1.3}$ keV, the measurement of the y-parameter of the S-Z effect gives

$$n_{e0} d_A = 1.50 \pm 0.12^{+0.22}_{-0.27} \times 10^{26} \text{ cm}^{-2} , \quad (17)$$

where the first error is due to statistical noise and the second is due to uncertainty in the electron temperature. We solve these two equations and find the central electron density, $n_{e0} = 5.64^{+0.72+1.44}_{-0.64-0.80} \times 10^{-2}$ cm^{-3} and $d_A = 867^{+189}_{-168}$ Mpc.

We can calculate H_0 for different cosmologies using the standard formula for angular diameter distance in Friedmann-Lemaitre cosmologies:

$$d_A = \frac{c}{H_0(1+z)\sqrt{\kappa}} \chi(x) , \quad (18)$$

where

$$x = \sqrt{\kappa} \int_0^z [(1+z')^2(1+\Omega_M z') - z'(2+z')\Omega_\Lambda] dz' . \quad (19)$$

For $\Omega_m = 1, \Omega_\Lambda = 0$, we find $H_0 = 59^{+16+35}_{-14-20}$, where the first error is from combination of statistical and systematic errors in the estimation of the X-ray and S-Z normalizations and the second error is from the uncertainty in the cluster gas temperature. For $\Omega_m = 0.3$, $\Omega_\Lambda = 0.7$ we find $H_0 = 66^{+21+38}_{-15-22}$.

5.2. *Additional Uncertainties*

In determining the error in the estimate of the Hubble constant and the cluster central electron density, we have considered both statistical errors in the measurements of the amplitude of S-Z and X-ray emission and additional uncertainties in the determination of the y-parameter and the Hubble constant due to deviations from spherical geometry, uncertainty in the average temperature of the gas, uncertainty in the cluster peculiar velocity, and astrophysical confusion. The contribution of each of these additional sources of uncertainty to y_0 and H_0 are listed in Tables 4 and 5, respectively. We describe some of these effects in detail.

5.2.1. *Relativistic Corrections*

At an electron temperature of 9.8 keV, relativistic corrections to the y-parameter calculation are significant. The SED of the relativistic S-Z effect has recently been estimated to high precision by several groups (Itoh, Kohyama, & Nozawa 1998; Challinor & Lasenby 1998). We use the parameterization of Itoh to calculate the S-Z spectrum for Abell 1835 over the range of electron temperatures determined from the X-ray observations, $8.5 < T_e < 12.1$ keV. The spectra of the extreme cases are shown in Figure 12. The allowed temperature range gives an error in the estimate of the y-parameter of $\pm 0.01 \times 10^{-4}$ due to relativistic corrections to the S-Z thermal spectrum.

The change in position of the S-Z null for different gas temperatures introduces different amount of S-Z thermal

TABLE 4

PEAK COMPTONIZATION AND CONTRIBUTIONS TO UNCERTAINTY USING THE BEST-FIT ISOTHERMAL MODEL

Source	Uncertainty ($y_0 \times 10^4$)
Statistical	4.9 ± 0.4
Baseline	± 0.13
Calibration	± 0.26
Position	$^{+0.06}_{-0.05}$
Density Model	$^{+0.07}_{-0.10}$
Peculiar Velocity	± 0.23
Radio Confusion	$^{+0.03}_{-0.01}$
Primary Anisotropies	± 0.11
Total	4.9 ± 0.6

TABLE 5

H_0 USING MASS-WEIGHTED TEMPERATURE FROM A MULTIPHASE MODEL AND X-RAY NORMALIZATION FROM *ROSAT* PSPC AND HRI IMAGES

Source	Uncertainty (km s^{-1} Mpc^{-1})
X-ray normalization	$^{+5.6}_{-5.3}$
S-Z normalization	$^{+15.4}_{-13.4}$
Central temperature	$^{+34.5}_{-20.3}$
Total	59^{+39}_{-28}

NOTE.—The S-Z normalization includes uncertainties due to statistical uncertainty, baseline, calibration, and astrophysical confusion.

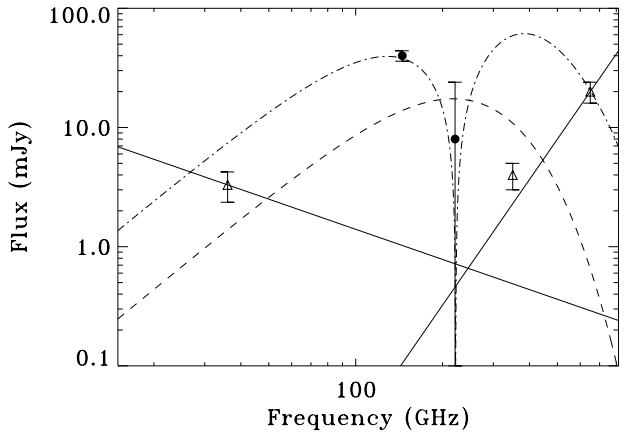

FIG. 12.—S-Z flux vs. frequency integrating the best-fit King model for the surface brightness of Abell 1835 over a 1.'7 FWHM Gaussian beam. Fluxes are from the S-Z thermal effect assuming an isothermal gas temperature of 9.8 keV and y-parameter of 4.9×10^{-4} (*dot-dashed line*) and from the kinematic effect assuming a peculiar velocity of 1000 km s^{-1} (*dashed line*). Solid circles are SuZIE measurements at 145 and 221 GHz. Open triangles are published point source fluxes for Abell 1835 (from Cooray et al. 1998 and Edge et al. 1999). The solid lines show extrapolations of the point source fluxes to millimeter wavelengths, using an index of $\alpha = 0.84$ for the radio emission and a graybody spectrum with $n = 1.5$ for the dust emission.

signal into the SuZIE peculiar velocity channel at $\nu = 221$ GHz. For the best-fit y-parameter of $y_0 = 4.9 \times 10^{-4}$ we calculate the residual thermal S-Z signal in the 1.4 mm channel as a function of electron temperature. We show the results of this calculation for the nonrelativistic S-Z effect and for the relativistic S-Z effect with electron temperatures of 8.5 and 12.1 keV in Table 6. The residual signals correspond to equivalent peculiar velocity signals smaller than 400 km s^{-1} for all channels over the range of electron temperatures determined from the X-ray observations of Abell 1835.

5.2.2. *Density Model Uncertainties*

The distribution of the electron gas in Abell 1835 at large distances from the cluster center is best measured by the *ROSAT* PSPC. Because the amplitude of the S-Z effect depends on the integrated electron density rather than the density squared, it is less sensitive to the central density enhancement from the cooling flow than to the parameters of the best-fit King model at large radii. We use the extreme values of β and θ_0 within the 68% contours from the fit of the King model to the PSPC data and calculate the change in S-Z normalization. The best-fit values are $\beta = 0.58 \pm 0.02$ and $\theta_0 = 0.'22^{+0.02}_{-0.02}$. However, the values of β and θ_0 are correlated with $\beta \sim \theta_0(\text{arcmin}) + 0.36 \pm 0.05$. We calculate $y_0 = 5.0 \times 10^{-4}$ for $\beta = 0.60$, $\theta_0 = 0.'20$ and $y_0 = 4.8 \times 10^{-4}$ for $\beta = 0.56$, $\theta_0 = 0.'24$ giving an error in the estimate of the y-parameter of $\Delta y_0 = \pm 0.1 \times 10^{-4}$ from density model uncertainties.

TABLE 6

RESIDUAL SIGNAL FROM THE S-Z THERMAL EFFECT IN THE 221 GHz CHANNELS OF SuZIE II

ELECTRON TEMPERATURE T_e	CHANNEL			
	2+	2−	5+	5−
nr	383	162	338	220
8.5 keV	42	−154	8	−99
12.1 keV.....	−172	−353	−202	−301

NOTE.—Signals are expressed in terms of an equivalent peculiar velocity signal in km s^{-1}.

5.2.3. *Deviations from a Spherical Gas Distribution*

Deviations from spherical geometry will generate S-Z amplitudes that are too high relative to the X-ray intensity if the long axis of the cluster is aligned with the line of sight or too low if the cluster is elongated perpendicular to the line of sight. Enhancement of the S-Z signal will produce an underestimate of the Hubble constant by $1 - \epsilon$, where ϵ is the cluster ellipticity (BHA). The orientation of a random sample of clusters should average to zero so that this error can be reduced with a large enough sample. However, in this era of first detections of the S-Z effect at millimeter wavelengths, experiments naturally target the brightest clusters in the X-ray, which can bias the sample toward clusters elongated along the line of sight and therefore low values of H_0. Cooray et al. (1998) point out that this effect should anticorrelate to the estimation of baryon fraction in clusters since the Hubble constant is proportional to

$$H_0 \propto \frac{1}{d_A Z}, \tag{20}$$

and

$$f_{\text{gas}} \propto \frac{d_A^{3/2}}{Z}, \tag{21}$$

where $Z = (1 - \epsilon(2 - \epsilon)\cos^2(\theta))^{1/2}$ and θ is the angle between the cluster main axis and the line of sight. If we assume that the anticorrelation between H_0 and f_{gas} in the cluster sample used by Cooray is due to variation in cluster ellipticity we find an error in the Hubble constant calculation with a rms of $\Delta H_0/H_0 = \epsilon_{\text{rms}} = 0.3$ assuming that clusters have values of Z distributed randomly between the maximum and minimum values from the 10 cluster sample. This value is similar to the average ellipticity for a large sample of clusters, $\bar{\epsilon} = 0.277$ (McMillian, Kowalski, & Ulmer 1989). X-ray and millimeter-wave measurements with improved angular resolution can reduce this error in individual clusters.

5.2.4. *Peculiar Velocity*

We can use the limits to the peculiar velocity determined from the multifrequency millimeter-wave measurements of Abell 1835 to estimate the error in y-parameter. For a peculiar velocity of 860 km s^{-1} the signal at 145 GHz is:

$$\Delta y_0(145\ \text{GHz}) \approx \frac{\Delta T}{T} = \frac{v_p}{c}\,\tau\,. \tag{22}$$

For Abell 1835, $\tau = y_0/(kT_e/m_e c^2) = 0.023$ so that the error in y_0 from the peculiar velocity limit is $\Delta y_0 \pm 0.77 \times 10^{-4}$. Cosmological models predict values of less than 300 km s^{-1} for the rms peculiar velocity of clusters of galaxies in a high density universe (Haehnelt & Tegmark 1996). The error in the y-parameter measurement due to this cluster peculiar velocity rms is on average $\Delta y_0 \pm 0.1(\tau/0.01) \times 10^{-4}$. We use this error in our final error budget. Measurements at lower frequencies in the Rayleigh-Jeans region of the CMB spectrum have $2y_0 = \Delta T/T$ and are half as sensitive to the effects of peculiar velocities.

TABLE 7

$f_{\rm gas}^{\rm S\text{-}Z}(r_{500})$ USING MASS-WEIGHTED TEMPERATURE FROM A MULTIPHASE MODEL, A BETA MODEL DENSITY DISTRIBUTION WITH $\beta = 0.58$, $\theta_0 = 0'.22$ FROM *ROSAT* PSPC AND HRI IMAGES AND S-Z NORMALIZATION

BARYON FRACTION AND UNCERTAINTY	
Source	Uncertainty
X-ray normalization	$^{+0.006}_{-0.005}$
S-Z normalization	$^{+0.018}_{-0.017}$
β	$^{+0.036}_{-0.029}$
r_0	$^{+0.028}_{-0.025}$
Central temperature	$^{+0.022}_{-0.028}$
Total	$0.155^{+0.054}_{-0.050}$

5.2.5. *Astrophysical Confusion*

Astrophysical confusion from randomly distributed sources is expected to be small at mm wavelengths (Fischer & Lange 1993); however, strong emission is often observed from dust and radio sources at the center of clusters with large cooling flows. A survey of X-ray selected clusters with $z < 0.1$ showed 71% of cD galaxies in X-ray clusters with central cooling flows had significant radio emission at 6 cm (Burns 1990). In this sample the radio brightness was observed to be correlated with both the accretion rate of the cooling flow, $\dot{M}$, and the pressure of the intracluster gas, $n_e kT_e$. Abell 1835 has both a large electron pressure, $n_{e0} kT_{e0} = 1.64 \times 10^{-10}$ dyn cm^{-2}, and one of the largest cooling flows observed in any cluster, $\dot{M} = 2000\ M_\odot$ yr^{-1}. Cooray et al. report the detection of a point source at the position of the central galaxy of A1835 at 28.5 GHz with a flux of 3.3 ± 0.9 mJy. Combining this measurement with data at 1.4 GHz (Condon, Dickey, & Salpeter 1990) gives a spectral index of $\alpha = 0.84$ (Cooray et al. 1998). Pointlike emission from Abell 1835 is also detected by *IRAS* at 60 μm and more recently by SCUBA at 450 and 850 μm with fluxes of 20 ± 4 mJy and 4 ± 1 mJy, respectively (Edge et al. 1999). Scaling these measurements to $\lambda = 2.1$ mm with a power-law spectral index gives a total flux limit of less than 1 mJy or $\Delta y_0 \leq -0.2 \times 10^{-4}$. We include this error in Table 5 under source confusion.

It is also possible for the measurement of the S-Z effect to be confused by the presence of primordial anisotropies of the CMB. The spectrum of these distortions is identical to that introduced by the S-Z kinematic effect and, therefore, especially serious for the determination of cluster peculiar velocities. Haehnelt & Tegmark (1996) have estimated the confusion limits from primary anisotropies to the determination of peculiar velocities. We can use their results to determine the effect of primary anisotropies on the measurement of the peak Comptonization. For $\Omega = 1$ (CDM) models with $\Omega_{\rm baryon} = 0.01 - 0.1$ and our beam size, $|\Delta v_{\rm pec}| < 300$ km s^{-1}. Therefore, primary anisotropies add an uncertainty of $\Delta y_0/y_0 = \pm 3.6\%$ to the peak Comptonization parameter in A1835.

6. BARYON MASS FRACTION

Most of the baryonic matter in galaxy clusters is in the X-ray emitting gas. The mass of this gas is equal to the integral of the gas density, which can be parameterized by a beta model:

$$M_g(r) = m_p \int_0^r 4\pi n_{e0}\, r^2 \left(1 + \frac{r}{r_c}\right)^{-3\beta/2} dr \qquad (23)$$

or a dark matter profile:

$$M_g(r) = m_p \int_0^r 4\pi n_{e0}\, r^2 (1 + x)^{\eta/x} dr\ , \qquad (24)$$

where $x = r/r_s$, $\eta = 4\pi G \rho_s r_s^2\, \mu m_p/(kT_{\rm gas})$ and $\rho_s = \rho_c\, \delta_c\, (1 + z)^3 \Omega_0/\Omega_s$ (Navarro, Frenk, & White 1997). The total mass within a radius, r is related to the temperature of the gas assuming hydrostatic equilibrium:

$$M_T(r) = \frac{3\beta}{G} \frac{kT_e r}{\mu m_p} \frac{(r/r_c)^2}{1 + (r/r_c)^2} \qquad (25)$$

The ratio of gas mass to total cluster mass can be estimated from measurements of the gas temperature T_e, spatial distribution, r_c, β, and density normalization, n_{e0}. In general, the gas fraction varies with cluster radius and values for different clusters are compared at a radius where the average density is 500 times the critical density:

$$\frac{3M_T(r_{500})}{4\pi r_{500}^3} = 500\, \frac{8\pi G}{H_0^2}\ . \qquad (26)$$

The gas fraction determined from a sample of over 200 clusters using data from X-ray measurements alone assuming a beta model density distribution is $f_{\rm gas}^{\rm X\text{-}ray}(r_{500}) = (0.120 \pm 0.004) h_{50}^{-3/2}$ (Cooray 1998b; Evrard, Metzler, & Navarro 1996). Recently the gas fraction has been estimated to be $f_{\rm gas}^{\rm X\text{-}ray}(r_{500}) = 0.168 h_{50}^{-3/2}$ with a 95% confidence range of 0.101 to 0.245 from an analysis of *ROSAT* PSPC data for 36 clusters using the dark matter density profile from Navarro et al. (Ettori & Fabian 1999). The same calculation has been made for 10 clusters using the S-Z flux to find the density normalization and gives values of $f_{\rm gas}^{\rm S\text{-}Z}$ ranging from $0.11/h_{50}$ to $0.25/h_{50}$ (Cooray et al. 1998). We find a baryon fraction for Abell 1835 assuming a beta model to be $f_{\rm gas}^{\rm S\text{-}Z}(r_{500}) = (0.155^{+0.054}_{-0.050}) h_{50}^{-1}$. The individual contributions to the error in this estimate from the uncertainty in the parameters r_c, β, T_X, and S-Z normalization, $n_{e0}\, d_A$, are given in Table 7. Using our best-fit normalization to the deprojected density profile from the *ROSAT* HRI image of Abell 1835 of $n_{e0}^2\, d_A = 8.47^{+0.67}_{-0.64} \times 10^{24}$ cm^{-5} we find $f_{\rm gas}^{\rm X\text{-}ray}(r_{500}) = (0.20 \pm 0.05) h_{50}^{-3/2}$.

These estimates depend on the accuracy of the assumption of hydrostatic equilibrium in the gas. Estimates of total mass from strong gravitational lensing in clusters agree well with the estimates from the X-ray emission temperatures and profiles for cooling flow clusters. However, high central density in cooling flow clusters can bias measurements to high values of gas fraction. To understand these systematic effects and place limits on cosmological matter density and cluster evolution it is important to obtain a sample of both X-ray and S-Z measurements for both cooling flow and noncooling flow clusters over a range of redshifts.

7. SUMMARY

We have presented observations of the cluster Abell 1835 with the SuZIE I receiver at 142 GHz and with the SuZIE II multifrequency array at 145, 221, and 279 GHz. We detect the Sunyaev-Zeldovich effect as a decrement in the intensity of the CMB with both receivers at 142 and 145 GHz. The

amplitude of the effect from both measurements agree within the statistical errors and provides a good check for systematic baseline effects. The combined y-parameter measurement is $y_0 = 4.9 \pm 0.6 \times 10^{-4}$. We have used the multifrequency data to place an upper limit on the peculiar velocity of Abell 1835 of $v_p = 500 \pm 1000$ km s^{-1}. Finally, we combine the millimeter-wave S-Z measurements with X-ray observations of Abell 1835 with the *ROSAT* and *ASCA* satellites to calculate a value for the Hubble constant of $H_0 = 59^{+38}_{-28}$ km s^{-1} Mpc^{-1}.

The S-Z effect has now been detected in many of the brightest X-ray clusters with both interferometers and single-dish observations at centimeter to submillimeter wavelengths (see Birkinshaw 1999 for a list of published results). The error in the estimate of the Hubble constant from statistical noise in these measurements is small compared to the estimated systematic errors. Additional data from SuZIE observations in a sample of $\sim$20 clusters is under analysis using the methods described in this paper. Future data from X-ray satellites such as *CHANDRA* and *ASTRO-E* can reduce the errors in the estimation of cluster gas temperatures and morphologies which dominate the uncertainty in the calculation of the Hubble constant. Future measurements of the S-Z effect from ground-based interferometers and single-dish telescopes will provide S-Z maps with high sensitivity and angular resolution comparable to the *ROSAT* images.

Thanks to the entire staff of the CSO for their excellent support during the observations. Thanks also to Barth Netterfield for helpful discussion regarding data analysis. The CSO is operated by the California Institute of Technology under funding from the National Science Foundation, contract AST-93-13929. This work has been made possible by a grant from the David and Lucile Packard foundation, by a National Science Foundation grant AST-95-03226 and by support from the LMT project for Mauskopf, sponsored by Advance Research Project Agency, Sensor Technology Office DARPA Order C134 Program Code 63226E issued by DARPA/CMO under contract MDA972-95-C-0004. This research has made use of data obtained through the High Energy Astrophysics Science Archive Research Center Online Service, provided by the NASA/Goddard Space Flight Center.

REFERENCES

Allen, S. W. 1997, preprint (astro-ph/9710217)
Allen, S. W., & Fabian, A. C. 1998, MNRAS, 297, L57
Allen, S. W., Fabian, A. C., Edge, A. C., Bautz, M. W., Furuzawa, A., & Tawara, Y. 1996, MNRAS, 283, 263
Birkinshaw, M. 1999, Phys. Rep., 310, 97
Birkinshaw, M., Hughes, J. P., & Arnaud, K. A. 1991, ApJ, 379, 466
Burns, J. O. 1990, AJ, 99, 14
Challinor, A., & Lasenby, A. 1998, ApJ, 499, 1
Church, S. E., Ganga, K. M., Holzapfel, W. L., Ade, P. A. R., Mauskopf, P. D., Wilbanks, T. M., & Lange, A. E. 1997, ApJ, 484, 523
Condon, J. J., Dickey, J. M., & Salpeter, E. E. A. 1990, AJ, 99, 1071
Cooray, A. A., Grego, L., Holzapfel, W. L., Joy, M., & Carlstrom, J. E. 1998, AJ, 115, 1388
Ebeling, H., Vogel, W., Bohringer, H., Edge, A. C., Huchra, J. P., & Briel, U. G. 1996, MNRAS, 281, 799
Edge, A. C., Ivison, R. J., Smail, I., Blain, A. W., & Kneib, J.-P. 1999, MNRAS, 306, 599
Ettori, S., & Fabian, A. C. 1999, preprint (astro-ph/9901304)
Evrard, A. E., Metzler, C. A., & Navarro, J. F. 1996, ApJ, 469, 494
Fabian, A. C., Hu, E. M., Cowie, L. L., & Grindlay, J. 1981, ApJ, 248, 47
Fischer, M. L., & Lange, A. E. 1993, ApJ, 419, 194
Haehnelt, M. G., & Tegmark, M. 1996, MNRAS, 279, 545
Hasinger, G., Turner, T. J., George, I. M., & Boese, G. 1992, OGIP Calibration Memo CAL/ROS/92-001 (Greenbelt: NASA)
Holzapfel, W. L., et al. 1997a, ApJ, 480, 449
Holzapfel, W. L., Ade, P. A. R., Church, S. E., Mauskopf, P. D., Rephaeli, Y., Wilbanks, T. M., & Lange, A. E. 1997b, ApJ, 481, 35
Holzapfel, W. L., Wilbanks, T. M., Ade, P. A. R., Church, S. E., Fischer, M. L., Mauskopf, P. D., Osgood, D. E., & Lange, A. E. 1997c, ApJ, 479, 17
Itoh, N., Kohyama, Y., & Nozawa, S. 1998, ApJ, 502, 7
Mauskopf, P. D., et al. 2000, ApJ, submitted
Mauskopf, P. D., Bock, J. J., Del Castillo, H., Holzapfel, W., & Lange, A. E. 1997, Appl. Opt., 36, 765
McMillian, L. W., Kowalski, M. P., & Ulmer, M. P. 1989, ApJ, 70, 723
Navarro, J. F., Frenk, C. S., & White, S. D. M. 1997, ApJ, 490, 493
Orton, G. S., Griffin, M. J., Ade, P. A. R., Nolt, I. G., Radostitz, J. V., Robson, E. I., & Gear, W. K. 1986, Icarus, 67, 289
Schlegel, D. J., Finkbeiner, D. P., & Davic, M. 1998, ApJ, 500, 525
Sunyaev, R. A., & Zeldovich, Ya. B. 1972, Comments Astrophys. Space Phys., 4, 173
Voges, W., et al. 1999, A&A, 349, 389